Sustainable recycling of intact carbon fibres from end-of-service-life composites

DOI:
10.1039/C9GC01847F

Document Version
Accepted author manuscript

Pi-yu CHEN, Chun PEI, Ji-Hua ZHU, Mei-ni SU (Corresponding author), Feng XING, (2019), "Sustainable recycling of intact carbon fibres from end-of-service-life composites", Green Chemistry, 21, 4757 - 4768.

Sustainable recycling of intact carbon fibres from end-of-service-life composites

Pi-yu CHEN[1§], Chun PEI[1§], Ji-Hua ZHU[1]*, Meini SU[1,2]*, Feng XING[1]

1 Guangdong Province Key Laboratory of Durability for Marine Civil Engineering, School of Civil Engineering, Shenzhen University, Shenzhen, Guangdong, China.

2 School of Mechanical, Aerospace and Civil Engineering. University of Manchester, Manchester, UK

[§]Pi-yu CHEN and Chun PEI contributed equally to this work.

* Corresponding authors: zhujh@szu.edu.cn (Ji-Hua Zhu), Meini.su@manchester.ac.uk (Meini Su)

ABSTRACT:

A novel method is developed to reclaim carbon fibres from carbon fabric-reinforced cementitious composites. The method takes advantage of an electrically driven chemical reaction in the presence of an aqueous electrolyte solution and an electrical current. This paper presents an experimental programme to investigate the effects of the applied current density, the sodium chloride and nitric acid concentrations in the solution and the temperatures. Both tensile strengths and interfacial shear strengths of the reclaimed carbon fibres were evaluated. Microstructural analyses on the morphologies of the reclaimed carbon fibres were also performed. The proposed method is simple, environmentally friendly and efficient. This method has no size limits on the recycled composites, which indicates the suitability of this approach for large-scale industrial applications. The reclaimed carbon fibres are found to be intact and believed to contain great commercial values since the recycling process did not damage their strengths or reduce their dimensions.

Keywords: Carbon fabric, Composites; Characterization; Electrochemical recycling

1. Introduction

Carbon fibre (CF) is a new kind of inorganic material with a multitude of advantages, such as light weight, high tensile strength, high stiffness, high corrosion resistance, and high temperature tolerance [1-4]. Since the late 1980s, carbon fibre-reinforced polymer (CFRP) plates/sheets have been used with epoxy resin to strengthen reinforced concrete structures in the construction industry in Europe, the US and Japan. Over the last 30 years, epoxy resin has become a popular bonding material due to its excellent bonding strength

[5-8]. However, the CFRP-epoxy resin strengthening system also has disadvantages, such as poor resistances to ageing, corrosion, moisture, heat, peeling, cracking and impacts. Therefore, new inorganic cementitious bonding materials (e.g., cement pastes and mortar) have begun to attract interest from industry, especially in the last decade. The advantages of cementitious materials include excellent corrosion resistances, outstanding mechanical properties, such as high strength and strong toughness, and great bonding characteristics with civil engineering structural materials [9].

The wide application of carbon fabric-reinforced cementitious matrix (C-FRCM) composites (i.e., CF cloths/plates/sheets/meshes embedded in a cementitious matrix) in the industry [10, 11] also creates substantial waste disposal issues. Moreover, end-of-service-life (EOSL) C-FRCM composites still contain CFs with high residual strengths and commercial values. Therefore, the recycling and reuse of CFs from EOSL composites not only alleviates the pollution from wastes but also makes full use of the CFs, which has an important economic value and social significance. However, it is difficult to decompose a cementitious matrix and reclaim CFs from these composites. There are a number of studies on recycling techniques for reclaiming CFs from CFRP-epoxy resin waste, including mechanical recycling [12, 13], pyrolysis [14, 15], chemical solvent decomposition [16-19], sub/supercritical chemical recycling [20-22], fluidized-bed processes [23-25] and electrochemical recycling [26, 27]. However, there is no research on CF recovery from C-FRCM composites; this study is the first to propose a recycling method to reclaim CFs from cementitious composites.

In this paper, a new recycling method based on an electrically driven chemical reaction is developed to reclaim CFs from C-FRCM composites. The proposed recycling process occurs in an acidic electrolyte solution with an applied current. During the electrochemical reaction, most of the calcium in the cement paste is dissolved, while the majority of silicon remains in the form of $SiO_2 \cdot nH_2O$ gel, leaving a porous corroded cement paste [28]. Finally, the cementitious material loses mechanical interlocking with CFs; thus, the reclaimed CFs (rCFs) are obtained. This paper first presents an experimental programme to investigate the effects of current density, sodium chloride (NaCl) concentration in the electrolyte solution, nitric acid (HNO_3) concentration and temperature on the recycling results. Second, tensile tests and interfacial shear strength (IFSS) tests are performed to assess the qualities of the rCFs. Third, microstructural analyses, including scanning electron microscopy (SEM), atomic force microscopy (AFM) and X-ray photoelectron spectroscopy (XPS), are performed to help understand the

electrochemical reaction mechanism and observe the surface morphologies of the rCFs. The recycling method is optimized regarding the recovery rate and residual strengths of the rCFs based on the experimental results and characterization techniques.

2. Experimental program

2.1 Materials and specimens

The CFRP sheets were Hitex-C300 (12k one-way woven cloth with an areal density of 300 g/m^2) from the Nanjing Haituo Composite Material Co. LTD. The ordinary Portland cement was PO42.5R grade purchased from China Resources Cement Holdings LTD. The chemical composition and physical properties of cement were listed in Table SI. 1 The silicon powder was from Shanghai Xikeng, and the redispersible powder was DY-5025 from Germany. The chopped CFs in the cementitious matrix were 3 mm long. NaCl and HNO_3 were purchased from the Xilong Chemical Company. The composition of the cementitious matrix is shown in Table 1.

The dimensions of the C-FRCM composite sample were 30 × 265 × 5 mm (width × length × thickness), as shown in Fig. 1. The layers of the cementitious matrix were approximately 2 mm thick. The specimen was divided into three regions: the test region to reclaim CFs, the protected region, which was insulated and waterproof, and the electrical connection region, which was connected to the external power supply. The manufacturing process for the C-FRCM composite specimens was conducted in accordance with industry standards.

2.2 Experimental parameters

The variables considered in the electrochemical recycling method include the current density, the NaCl concentration in the electrolyte, the HNO_3 concentration and the temperature. To study the effects of each parameter, two series of experiments were designed in this study. The specimens were labelled according to the reaction conditions. For example, the specimen label "I20S2H3T40" comprises four parts: the first part, "I20", represents the applied current (20 mA, corresponding to 3.33 A/m^2); the second part, "S2", indicates the NaCl concentration in the electrolyte (2% of the weight of deionized water); the third part, "H3", refers to the HNO_3 concentration in the electrolyte (3 g/L); and the last part, "T40", indicates the temperature (40°C) at which the recycling process was performed.

In the first series of tests (Table 2), two current densities (3.33 and 6.67 A/m^2), two NaCl concentrations (2% and 3%) and four (HNO_3) concentrations (0, 1, 3 and 5 g/L) were considered. A total

of 16 reaction conditions were included in the test programme, and three samples were used for each set of reaction conditions. In the second series of tests in the experimental programme (Table 3), the effect of temperature was considered. Two reaction conditions with the best performance were selected from the first series of tests. Therefore, the variables considered in the second series of recycling conditions include (1) two applied current densities (20 mA and 40 mA, which correspond to 3.33 A/m^2 and 6.67 A/m^2, respectively), (2) one NaCl concentration (2%), (3) one HNO_3 concentration (3 g/L) and (4) three temperatures (40°C, 60°C and 75°C). A total of six reaction conditions were considered, and three specimens were used for each set of reaction conditions.

2.3 Recycling process

The experimental device used for the CF recycling process is shown in Fig. 2. The recycling device consists of four main parts: (1) a DC power supply, which provides current to the system; (2) a cathode and an anode, wherein the specimen was connected to the positive pole of the power supply and a stainless steel plate was connected to the negative pole of the power supply as the cathode with 50 mm distance between the two electrodes is in the experimental programme; (3) an electrolyte, which consisted of NaCl and HNO_3 solution; and (4) a datalogger, which monitored the voltage changes in the system. The first series of electrochemical reactions at room temperature lasted for 8 days, while the second series of reactions at elevated temperatures lasted for 4 days. Afterwards, the specimens (Fig. 3(a)) were cleaned by loosening the cementitious matrix by pressing holes on the surface of the cementitious matrix (Fig. 3(b)) and flushing with a water pressure of 0.5 MPa for 10 seconds (Fig. 3(c)). The cleaned rCFs are shown in Fig. 3(d).

2.4 Mechanical tests of the rCFs

The properties of the rCFs were evaluated based on the voltage monitoring of the recovery process by a datalogger (HIOKI-LR8400, Japanese Nikko electric corporation), the hardness tests of the composites after the electrochemical reactions, the tensile tests of the rCF monofilaments, and the IFSS tests between the rCFs and epoxy resin.

The hardness of the composite plate was tested after the recycling process with a coated pencil [29]. According to the specifications, the composite was kept dry, placed on a flat desk and pressed with the pencil under a load of 7.5 N at a direction of 45°; the loading rate was 0.5–1 mm/s. Pencils of different grades from 9B (softest level) to 9H (hardest level) were pressed onto the composite surface.

The hardness of the composite surface was measured starting from the softest pencil and determined when a visible mark occurred.

The tensile strength of a CF monofilament was tested with a UTM-Bionix Standard Toecomp Quasistatic test system. The loading rate in the tensile test was 0.2 μm/s, and the CF sample length was 6 mm. According to ISO 11566 [30], a total of 20 samples were tested for each reaction condition. Before testing, the diameter of the CF monofilament was measured with a laser calliper (Changchun Industrial Optoelectronic Technology Co. LTD).

The IFSS between a CF monofilament and epoxy resin was determined by the microdroplet test using an HM410 composite interfacial evaluation device (Japanese Tongrong Corporation). Before testing, the diameter of each resin microdroplet was measured by a high-resolution microscope built in the test system. According to previous studies [31], the diameter of the resin microdroplet was 40–80 μm. A total of five parallel tests were conducted for each reaction condition. The loading rate for the IFSS test was 0.12 mm/min.

2.5 Instrumentation

The microstructures of the rCFs were analysed by means of SEM, AFM and XPS. The effects of the reaction conditions on the mechanical properties of the rCFs were explained at a microscopic scale. A Quanta TM 250 FEG scanning electron microscope (FEI company, USA) was used in this study. The scanning environment was in high-vacuum mode, the working distance was approximately 10 mm, and the test acceleration voltage was 20 kV. To improve the conductivity of the CF, the sample was first prepared with a gold spray before testing. AFM technology (ICON-PT-PKG, Brooker company, USA) was used to scan the surface topographies of the rCFs. The scanning range of the sample was 4 μm× 4 μm, as suggested by Guo [32], and the scanning speed was 1.0 Hz. NanoScope Analysis 1.8 was used to analyse the images and quantify the rCF surface roughness.

The XPS technology (ULVAC-PHI VPII photoelectron spectrometer) was used to analyse the type and content of the elements and functional groups on the surfaces of the rCFs. Using the XPS Peak 4.1 software, the results were fitted with a Gaussian function and a Lorentz function to obtain the information of the functional groups. The X-ray source of the monochromator was an Al target. The rCFs were scanned in full spectrum before C_{1s} was scanned in a high-resolution narrow spectrum. The incident angle was 90°.

3. Results and discussion

In this part, the effects of the current density, NaCl concentration, HNO_3 concentration and temperature on the CF recovery are discussed from the perspectives of system voltage, recycling amount, mechanical properties and microstructures of the rCFs.

3.1 System voltage

During the electrochemical recycling process, the measured voltages under different reaction environments were generally stable, as shown in Fig. 4(a). In general, the voltages of the recycling system under a 40 mA current were larger than those under a 20 mA current. The voltages under an NaCl concentration of 3% were larger than those under an NaCl concentration of 2%. The voltages of the reaction condition without HNO_3 were found to be higher than those under the reaction conditions with HNO_3. These phenomena can be explained by the slow degradation of the cementitious matrix in the absence of HNO_3 and the high electrical resistance of the composite. The voltages under the reaction conditions with a high HNO_3 concentration (5%) were also relatively high because both the cementitious matrix and CF were damaged in this environment. The voltages under the reaction conditions where the HNO_3 concentrations were either 1% or 3% were the lowest among all considered conditions. Under elevated temperature conditions, the measured voltages of all specimens were generally stable during the recycling process. The voltage differences of the specimens under different parameters and conditions were very small, as shown in Fig. 4(b). The voltage fluctuations of the specimens in the I20 series were less than 0.15 V, and those of the specimens in the I40 series were less than 0.10 V. The measured voltages of the specimens at 60°C were the lowest, indicating the good electrical conductivity of the system and low damage to the rCFs.

3.2 Recycling amount

The weight of the virgin CF (vCF) sheet was 841 mg. In the absence of the HNO_3 solute, no rCFs were obtained since the composite was still hard and the cementitious matrix could not be removed. As shown in Table 4, in the presence of the HNO_3 solute, the number of rCFs increased with increasing HNO_3 concentration in the beginning and then decreased. When the HNO_3 concentration was 3 g/L, the greatest number of rCFs was collected, and the current densities and NaCl concentrations had limited influences on the results. The greatest number of rCFs was collected at a reaction temperature of 40°C (91.8% of the vCFs). Note that the length of the recycling process under a high temperature was only half of that at

room temperature. Some researchers [20, 21, 33-35] also found similar conclusions, wherein reasonably high temperatures had beneficial effects on the chemical reclamation of CFs. At the same temperature, a greater number of rCFs was collected under a 20 mA current than under a 40 mA current.

3.3 Mechanical properties

The hardness values of the degraded C-FRCM composites after electrochemical recycling at either room temperature or higher temperatures are shown in Table 4. The concentration of the HNO_3 solute had the most substantial influence on the hardness, wherein the higher the concentration is, the more extensive the degradation and the lower the hardness value. Under the same concentration of the HNO_3 solute, a larger NaCl concentration and current resulted in a softer specimen surface. In the absence of the HNO_3 solute, the composite was only partly softened. The hardness of the treated composite directly affected the number of rCFs because it was easier to clean and collect a greater number of rCFs in the softer specimens. Temperature plays an important role in the degradation of the cementitious matrix. Similar to the findings at room temperature, the lower hardness values resulted in a greater number of rCFs.

The diameters of both the vCF monofilament and rCF monofilament were measured to be 7 μm, indicating that the rCFs had not been substantially degraded in the electrochemical recovery process. The tensile strengths of the rCFs are shown in Table 5 (also refer to Fig. SI2, SI3, Table SI2, SI3 and SI4). The tensile strength of the vCF was 3.58 GPa. The residual tensile strengths of the rCFs decreased as the HNO_3 concentration increased, indicating that the presence of HNO_3 might cause unfavourable degradation in the rCFs. The current density and NaCl concentration had limited effects on the tensile strengths of the rCFs. The diameters of the rCF filaments were found to be 7 μm, which were the same as those of the rCFs obtained at room temperature. The tensile strengths of the rCFs showed an increasing trend with increasing temperature. Generally, the tensile strengths of the CFs reclaimed under the 20 mA current condition were higher than those reclaimed under the 40 mA current condition. The highest residual tensile strength of the rCF was found to be 3.21 GPa (specimen I20S2H3T75), which was 89.58% of tensile strength of the vCF. The roughness values of the rCFs measured by AFM and the IFSS values between the rCFs and epoxy resin are shown in Table 5 and Fig. 8. When the temperature was 40°C, the rCFs were only slightly affected by the electrochemical reaction (Fig. 8(c)), and the roughness of the rCF was 134 nm, which is similar to the roughness of the vCF (144 nm). Thus, the IFSS values of the rCFs obtained at 40°C were relatively low. The greatest obtained IFSS value at 40°C was 28.45 MPa

(105.02% of the IFSS of the vCF). As the temperature continued to increase to 60°C, the grooves on the surfaces of the rCFs became deeper and more pronounced; in addition, both the amount and size of the convex hills increased (Fig. 8(d)). The roughness of the rCF at 60°C was found to be 168 nm. The changes in the topographies of the rCFs enhance the mechanical interlocking between the CFs and epoxy resin. The specimen I20S2H3T60 had the greatest IFSS value at 60°C. When the temperature reached 75°C, the grooves widened (Fig. 8(e)), and the roughness increased to 184 nm. However, the IFSS decreased under this condition. This decreasing phenomenon occurs due to the decreased mechanical bonding resulting from significant changes in the surface topography and the degraded chemical bonding resulting from fewer strong-hydrophilic group O-C=O bonds. In the IFSS tests, the failure modes of all specimens were debonding at the resin layer (DB) except specimen I40S2H3T60, whose failure mode was debonding at the interface between the CFs and the matrix (CB).

One of the most common applications of rCFs is for remanufacturing CFRPs with epoxy resins. Therefore, the IFSS between rCF and epoxy resin is one of the assessment criteria used for rCFs. Table 5 shows the IFSS between rCF and epoxy resin, and Fig. 7 shows the failure modes, which were observed via SEM. The IFSS between the vCF and epoxy resin was found to be 27.09 MPa, and the failure mode was DB (Fig. 7(a)). Generally, the IFSS values between the rCFs and epoxy resin decreased with increasing HNO_3 concentration. In the presence of a low concentration of HNO_3 (i.e., 1 g/L and 3 g/L), the IFSS between the rCF and epoxy resin was greater than that between the vCF and epoxy resin. When the HNO_3 concentration was 1 g/L and 3 g/L, smaller current densities and lower NaCl concentrations had positive effects on the rCFs. When the concentration of HNO_3 was 1 g/L, the failure mode of the rCF was similar to that of the vCF, which was a DB failure with a thin layer of epoxy resin on the surface of the rCF. The results indicate that the interface between the CF and epoxy resin was stronger than that between the epoxy resin layer. When the concentration of HNO_3 became 3 g/L, a CB failure was observed (Fig. 7(b)), showing that the weakest part of the specimen was the interface between the CF and epoxy resin. However, the IFSS values of the H3 series of specimens were still higher than that of the vCF, which might be attributed to the needle-like resin structures on the fracture surfaces. The needle-like structures could increase the contact area and roughness of the interfacial region between the CF and epoxy resin [36], thus leading to a greater IFSS.

3.4 Microstructures

SEM scanning was performed on a cementitious matrix to explore the degradation mechanism of the cementitious matrix during the electrochemical reaction. Fig. 5(a) shows the interface between cementitious materials and CF in the virgin specimen. The ribbed groove structures with regular shapes and some interpenetrating networks formed by the cement slurry and polymer throughout the structures were observed, which are similar to those found in the literature [37, 38]. These structures formed strong mechanical interlocking with CFs. The interface of the cementitious matrix and CF was changed after the electrochemical reaction (Fig. 5(b)). The diamond shape groove structure was cut off by large vertical and horizontal cracks into small broken units, and the porosity of the material was increased dramatically. Therefore, the interfacial mechanical interlocking between the cementitious matrix and CF was weakened. Some white colour products formed at the interface, which was speculated to be SiO_2 gel degraded from C-S-H gel [28, 39]. The mechanism can be explained by the leaching of Ca^{2+} ions in the cement matrix during electrochemical reaction, leading to the dissolution of $Ca(OH)_2$ and calcium sulphoaluminates. Porous structure formed after the decalcification of C-S-H in cement paste [28]. The CF was thus isolated from the cement matrix. A typical SEM image of rCFs reclaimed at high temperature condition is presented in Fig. 6(c) (Fig. SI6). The surface of rCFs reclaimed at high temperature was rather clean without visible cement gel particles and defects, which were different from rCFs reclaimed under room temperature (Fig. 6(b)). The reason may be that the recycling process under the high temperatures was shortened, which effectively reduced the degradation (oxidation and acidification, etc.) of rCFs.

Two typical pictures of the vCFs and rCFs (from specimen I40S2H3) are presented in Fig. 6. The surfaces of the vCFs were rather smooth without visible defects (Fig. 6(a)). The surfaces of the rCFs had some cement gel particles and clear longitudinal and horizontal cracks (Fig. 6(b)). The SEM images show the degradation of the rCFs, which explains the decrease in the residual tensile strength. In addition, the rCFs obtained under 20 mA current conditions had fewer defects compared to those obtained under 40 mA current conditions, indicating that the degradation of the CFs was caused by large currents.

Fig. 8 shows two typical AFM images of the vCFs and rCFs. The surfaces of the vCF were smooth and neat (Fig. 8(a)), whose roughness was found to be 144 nm. Due to oxidation etching during the electrochemical reaction, longitudinal grooves and convex hills along the fibre were formed on the surfaces of the rCFs (Fig. 8(b)). These changes to the fibre geometries significantly enhanced the

mechanical interlocking between the rCFs and epoxy resin, which are similar to the ribs in steel reinforcements used to improve the bonding between reinforcement and concrete. Moreover, the increasing roughness enhanced the bonding between the rCFs and epoxy resin. The relationship between the roughness and IFSS is shown in Fig. 9, wherein the IFSS generally increases as the rCF surface roughness increases. Therefore, rCFs could reach higher IFSS values than vCFs. In summary, when the HNO_3 concentration was low, mild oxidation etching during electrochemical recovery had a positive influence on the IFSS; when the HNO_3 concentration increased to a certain extent, excessive oxidation etching reduced the IFSS.

The full spectrum of the XPS scan and the high-resolution narrow spectrum of C_{1s} of the rCFs are shown in Fig. 10. There were five peaks observed in the full spectrum of scanning: the two main peaks were carbon(C) (284.6 eV) and oxygen(O) (532.0 eV), and the three secondary peaks were silicon (Si) (99.5 eV), chlorine (Cl) (199.8 eV) and calcium (Ca) (347 eV). The basic elements on the surfaces of the rCFs were C and O, and small amounts of Si, Cl and Ca were introduced during the recycling process. The elemental contents on the surfaces of vCF and rCF (I20S2 series) are shown in Table 6. The carbon and oxygen contents on the surface of the vCF were 79.3% and 20.7%, respectively. The carbon content on the rCF surface was approximately 10% less than that on the vCF surface, while the oxygen content was higher on the rCF surface. When the HNO_3 concentration was 3 g/L, the oxygen/carbon (O/C) ratio was found to be highest, indicating that in this reaction condition, the most oxygen had been introduced to the surface of the rCF, which led to greater surface activity and enhanced the chemical bonding between the rCF and epoxy resin [40, 41].

The XPS Peak 4.1 programme was used to classify the C_{1s} high-resolution narrow spectrum according to the binding energy into the following six bond peaks for Gaussian-Lorentz fitting: graphite state C-C (284.4 eV), amorphous state C-C (284.8 eV), C=O (285.5 eV), C-O (286.2 eV), C-Cl (287.2 eV) and O-C=O (288.4 eV) [33, 42-44]. The fitting of the C_{1s} split peaks is shown in Fig. 10, and the specific contents of the functional groups on the surface of the rCF are shown in Table 6. The results revealed that there were more carbon and oxygen-containing functional groups on the surface of the rCF than on the surface of the vCF. Studies have shown that in electrochemical anodization [34], the activated carbon and oxygen-containing functional groups on the surface of a CF can be gradually oxidized by oxygen atoms or ions: from C-O to C=O to O-C=O. The CFs reclaimed in this study were oxidized during the recovery

process, and the surface oxygen content increased, which enabled the surface to be more active. Moreover, the occurrence of hydrophilic O-C=O groups also greatly improved the chemical bonding between the rCFs and epoxy resin. The contents of the elements on the surfaces of the rCFs are shown in Table 6. Compared to the vCF, the content of carbon (C) decreased, and the oxygen (O) content substantially increased. The oxygen/carbon (O/C) ratio was found to be 0.2610 for the vCF and 0.407–0.429 for the rCFs. A large amount of active oxygen was incorporated onto the surfaces of the rCFs during the electrochemical process at high temperatures, which led to more oxygen-containing groups on the surfaces of the rCFs and a greater degree of oxidation.

The contents of the functional groups of C on the surfaces of the rCFs are shown in Table 6. The number of strong-hydrophilic group O-C=O bonds decreased at high temperatures because C tends to generate carbon dioxide and water at high temperatures [35]. This might explain the lower IFSS values of the rCFs at 75°C. The experimental results in this study indicated that increasing the temperature could increase the oxidation degree on the surfaces of the rCFs; however, if the temperature exceeds a certain threshold, over-oxidation would lead to a lower amount of rCFs and weaken the chemical bonding between the CF and cement matrix. In addition, the percentage of C-Cl bonds on the surface of specimen I20S2H3T40 was 8.2% (Table 6), showing that the rCFs obtained from this reaction condition were chlorinated, which resulted in decreased tensile strengths. However, it should be noted that the chlorine on the surfaces of the rCFs from specimens I20S2H3T60 and I20S2H3T75 were not in the chemical bonds (Table 6) but exists only in the adsorption state.

4. Conclusions

A new electrochemical method for recycling CFs from C-FRCM composites was developed in this study. This new method takes advantage of an electrically driven chemical reaction in the presence of an aqueous electrolyte solution and an electrical current. Furthermore, this recycling method used affordable and non-toxic chemicals, small currents and easily implemented facilities to reclaim intact CFs. Tensile tests and IFSS tests were conducted to characterize the rCFs. Microstructural analysis technologies were adopted to understand the mechanisms of the behaviours of the rCFs. The effects of different parameters were investigated by an experimental programme to optimize the recycling process. Experimental results showed that a low current density (3.33 A/m^2) and a low NaCl concentration (2%) could improve the electrochemical corrosion of the cement matrix and the tensile strengths of the rCFs. Adding an

appropriate amount of nitric acid (3 g/L) can enhance the recycling efficiency and the IFSS values between the rCFs and epoxy resin. Compared to normal temperature conditions, higher temperatures can further improve the recycling efficiency and the tensile strengths of the rCFs. The rCFs and vCFs exhibited similar properties: the residual tensile strengths of the rCFs were approximately 90% of that of the vCFs, the IFSS values of the rCFs were 117% of that of the vCFs, and the recovery of the rCFs was 92%. This new recycling method is expected to solve EOSL composite waste problems and fully utilize the residual values of disposed CFs. Because of the high-quality of the rCFs, they can also be used in various applications, ranging from aerospace to ground transportation, construction industries to sporting goods. Compared with traditional recycling methods, this new method is efficient, sustainable, inexpensive, and easily implemented, and the new method has no size limits on the recycled composites. Thus, this new recycling method is suitable for large-scale applications in industry.

Acknowledgements

The authors wish to express their gratitude and sincere appreciation to the National Natural Science Foundation of China (51861165204, 51778370, 51538007) and Natural Science Foundation of Guangdong (2017B030311004) and the Shenzhen Science and Technology Project (JCY20170818094820689) for financing this research work.

Declarations of interest

None.

References

[1] Park SJ, Kim BJ. Carbon Fibers and Their Composites: Springer Netherlands; 2015.

[2] Park SJ, Bae KM. Testing of Carbon Fibers and Their Composites: Springer Netherlands; 2015.

[3] Park SJ. Novel Carbon Fibers and Their Composites. Springer. 2018;210:275-317.

[4] Zhu J-H, Wei L, Moahmoud H, Redaelli E, Xing F, Bertolini L. Investigation on CFRP as dual-functional material in chloride-contaminated solutions. Construction and Building Materials. 2017;151:127-37.

[5] May C. Epoxy resins: chemistry and technology: CRC press; 1987.

[6] Czaderski C, Martinelli E, Michels J, Motavalli M. Effect of curing conditions on strength development in an epoxy resin for structural strengthening. Composites Part B: Engineering. 2012;43(2):398-410.

[7] Zhou Y, Fan Z, Du J, Sui L, Xing F. Bond behavior of FRP-to-concrete interface under sulfate attack: An experimental study and modeling of bond degradation. Construction and Building Materials. 2015;85:9-21.

[8] Zhou Y, Hu J, Li M, Sui L, Xing F. FRP-confined recycled coarse aggregate concrete: Experimental investigation and model comparison. Polymers. 2016;8(10):375.

[9] ACI. Guide to design and construction of externally bonded fabric-reinforced cementitious matrix (FRCM) systems for repair and strengthening concrete and masonry structures. 2013.

[10] Su M, Wei, L, Zhu, J.H., Ueda T., Guo G. and Xing, F. Experimental investigation of the ICCP-SS technique based on the C-FRCM composite. Journal of Composites for Construction, ASCE. 2019; 23(4):04019021.

[11] Zhu J.H., Su M.N., Huang J.Y., Ueda T, Xing F. The ICCP-SS technique for retrofitting reinforced concrete compressive members subjected to corrosion. Construction and Building Materials. 2018;167:669-79.

[12] Palmer J, Ghita OR, Savage L, Evans KE. Successful closed-loop recycling of thermoset composites. Composites Part A Applied Science & Manufacturing. 2009;40(4):490-8.

[13] Pickering SJ. Recycling technologies for thermoset composite materials—current status. Composites Part A Applied Science & Manufacturing. 2006;37(8):1206-15.

[14] Nahil MA, Williams PT. Recycling of carbon fibre reinforced polymeric waste for the production of activated carbon fibres. Journal of Analytical & Applied Pyrolysis. 2011;91(1):67-75.

[15] Cunliffe AM, Jones N, Williams PT. Recycling of fibre-reinforced polymeric waste by pyrolysis: thermo-gravimetric and bench-scale investigations. Journal of Analytical & Applied Pyrolysis. 2003;70(2):315-38.

[16] Jiang J, Deng G, Chen X, Gao X, Guo Q, Xu C, et al. On the successful chemical recycling of carbon fiber/epoxy resin composites under the mild condition. Composites Science and Technology. 2017;151:243-51.

[17] Wang Y, Cui X, Ge H, Yang Y, Wang Y, Zhang C, et al. Chemical Recycling of Carbon Fiber Reinforced Epoxy Resin Composites via Selective Cleavage of the Carbon–Nitrogen Bond. Acs Sustainable Chemistry & Engineering. 2015;3(12).

[18] Nie W, Liu J, Liu W, Wang J, Tang T. Decomposition of waste carbon fiber reinforced epoxy resin composites in molten potassium hydroxide. Polymer Degradation & Stability. 2015;111:247-56.

[19] Li J, Xu PL, Zhu YK, Ding JP, Xue LX, Wang YZ. A promising strategy for chemical recycling of carbon fiber/thermoset composites: self-accelerating decomposition in a mild oxidative system. Green Chemistry. 2012;14(1):3260-3.

[20] Piñero-Hernanz R, Dodds C, Hyde J, García-Serna J, Poliakoff M, Lester E, et al. Chemical recycling of carbon fibre reinforced composites in nearcritical and supercritical water. Composites Part A. 2008;39(3):454-61.

[21] Piñero-Hernanz R, García-Serna J, Dodds C, Hyde J, Poliakoff M, Cocero MJ, et al. Chemical recycling of carbon fibre composites using alcohols under subcritical and supercritical conditions. Journal of Supercritical Fluids. 2008;46(1):83-92.

[22] Bai Y, Wang Z, Feng L. Chemical recycling of carbon fibers reinforced epoxy resin composites in oxygen in supercritical water. Materials & Design. 2010;31(2):999-1002.

[23] Jiang G, Pickering SJ, Walker GS, Wong KH, Rudd CD. Surface characterisation of carbon fibre recycled using fluidised bed. Applied Surface Science. 2008;254(9):2588-93.

[24] Pickering SJ, Kelly RM, Kennerley J, Rudd C, Fenwick N. A fluidised-bed process for the recovery of glass fibres from scrap thermoset composites. Composites Science and Technology. 2000;60(4):509-23.

[25] Yip HLH, Pickering SJ, Rudd CD. Characterisation of carbon fibres recycled from scrap composites using fluidised bed process. Plastics, Rubber and Composites. 2002;31(6):278-82.

[26] Zhu J.H., Chen, P.Y., Su, M.N., Pei, C, Xing, F., Recycling of Carbon Fibre Reinforced Plastics by Electrically Driven Heterogeneous Catalytic Degradation of Epoxy Resin. Green Chemistry. 2019; 21:1635-1647.

[27] Sun H, Guo G, Memon SA, Xu W, Zhang Q, Zhu J-H, et al. Recycling of carbon fibers from carbon fiber reinforced polymer using electrochemical method. Composites Part A: Applied Science and Manufacturing. 2015;78:10-7.

[28] Shi C, Stegemann JA. Acid corrosion resistance of different cementing materials. Cement & Concrete Research. 2000;30(5):803-8.

[29] IX-ISO. Paints and varnishes - Determination of film hardness by pencil test 2012.

[30] IIX-ISO. Carbon fibre-determination of the tensile properties of single-filament specimens. 1996.

405 [31] Lei C, Zhao J, Zou J, Jiang C, Li M, Zhang X, et al. Assembly Dependent Interfacial Property of
406 Carbon Nanotube Fibers with Epoxy and Its Enhancement via Generalized Surface Sizing. Advanced
407 Engineering Materials. 2016;18(5):839-45.
408 [32] Guo H. Characterization of Surface Energy, Surface Roughness and Chemical Component of Carbon
409 Fibres. PhD thesis, Harbin Institute of Technology. 2009.
410 [33] Tian S, Li L, Sun W, Xia X, Han D, Li J, et al. Robust adhesion of flower-like few-layer graphene
411 nanoclusters. Sci Rep. 2012;2(7):511.
412 [34] Liu HP, Lv C.X., Li, Y.H., Yang, Y., Li, K.X. and He F. Surface properties of electrochemically
413 oxidized PAN-based carbon fibres. New Carbon Materials. 2005;20(1):39-44.
414 [35] Pimenta S, Pinho ST. The effect of recycling on the mechanical response of carbon fibres and their
415 composites. Composite Structures. 2012;94(12):3669-84.
416 [36] Zhang X FX, Yan C, et al. Interfacial microstructure and properties of carbon fibre composites
417 modified with graphene oxide. ACS applied materials & interfaces. 2012;4(3):1543-52.
418 [37] Y O. Principle of latex modification and some typical properties of latex-modified mortars and
419 concretes adhesion; binders (materials); bond (paste to aggregate); carbonation; chlorides; curing;
420 diffusion. Materials Journal. 1987;84(6):511-8.
421 [38] Isenburg JE, Vanderhoff JW. Hypothesis for Reinforcement of Portland Cement by Polymer Latexes.
422 Journal of the American Ceramic Society. 2010;57(6):242-5.
423 [39] Pavlík V. Corrosion of hardened cement paste by acetic and nitric acids part II: formation and
424 chemical composition of the corrosion products layer. Cement and Concrete research. 1994;24(8):1495-
425 508.
426 [40] Yue Z.R. Jiang W, Wang L., Gardner S.D., PittmanJr. C.U., Surface characterization of
427 electrochemically oxidized carbon fibers. Carbon. 1999;37(11):1785-96.
428 [41] Severini F, Formaro L, Pegoraro M, Posca L. Chemical modification of carbon fiber surfaces.
429 Carbon. 2002;40(5):735-41.
430 [42] Miao L, Feng C, Zhang Z, Lei X, Chen R, Yang Y, et al. Simultaneous reduction of nitrate and
431 oxidation of by-products using electrochemical method. Journal of Hazardous Materials.
432 2009;171(1):724-30.

[43] Rajeshwar K IJG. Environmental electrochemistry: Fundamentals and applications in pollution sensors and abatement. Elsevier. 1997.

[44] Heremans J, Rahim I, Dresselhaus MS. Thermal Conductivity and Raman Spectra of Carbon Fibers. Physical Review B Condensed Matter. 1985;32(10):6742-7.

List of figures

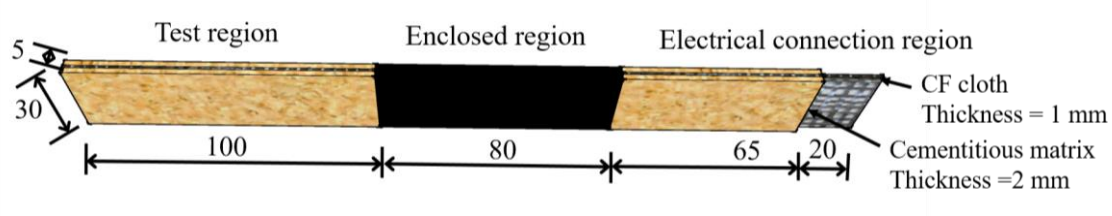
Test region
Enclosed region
Electrical connection region
5
30
100
80
65
20
CF cloth
Thickness = 1 mm
Cementitious matrix
Thickness =2 mm

Fig. 1.

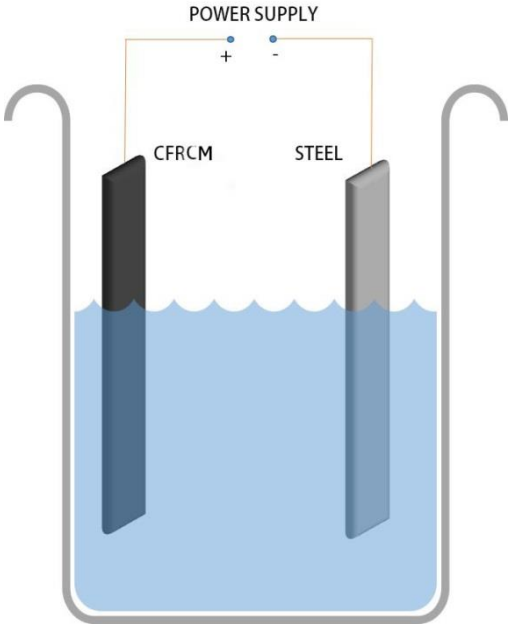
POWER SUPPLY
+
-
CFRCM
STEEL

Fig. 2.

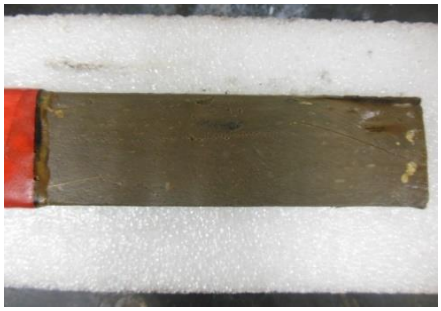

(a) After electrochemical reaction

(b) Loosen the cementitious matrix

(c) After flushing

(d) Cleaned rCFs

Fig. 3.

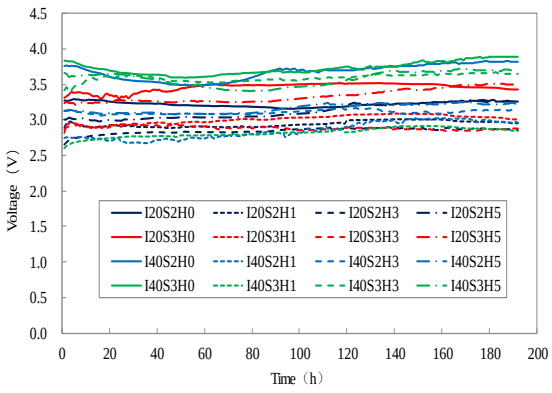

(a) First series

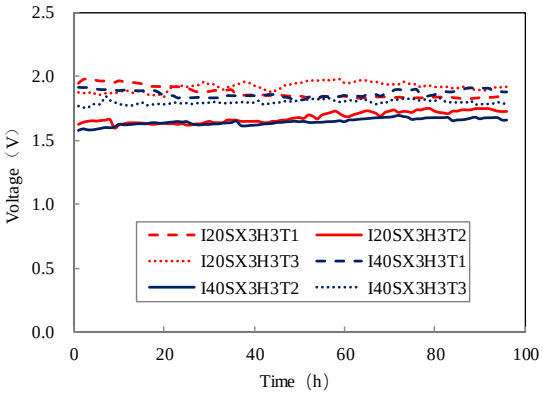

(b) Second series

Fig. 4.

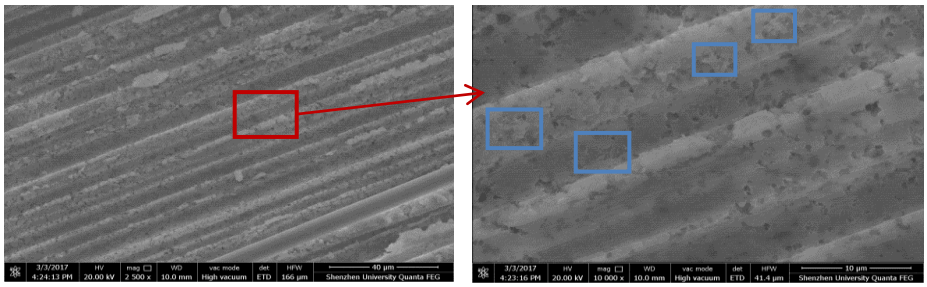

(a) Untreated composite board

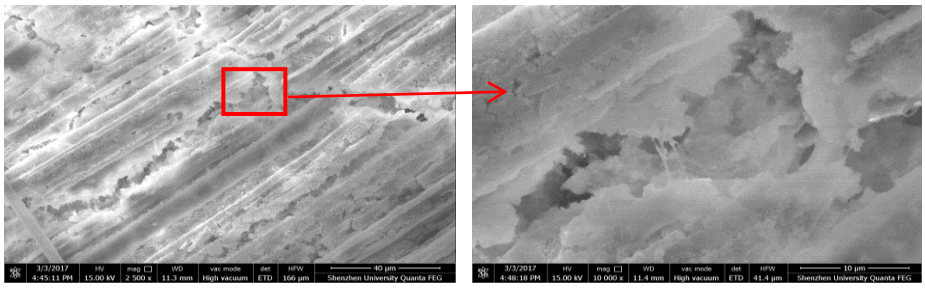

(b) Specimen I40S3H1

Fig. 5.

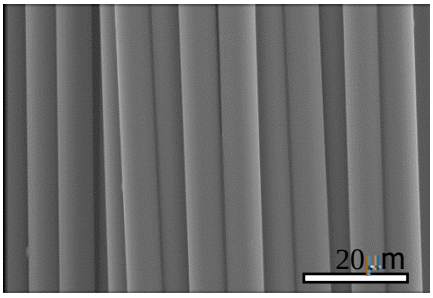

(a) vCF

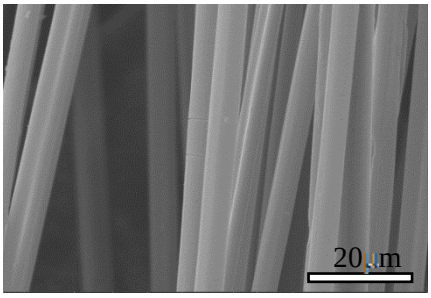

(b) Specimen I40S2H3

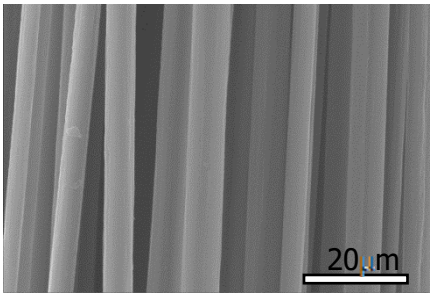

(c) Specimen I40S2H3T40

Fig. 6.

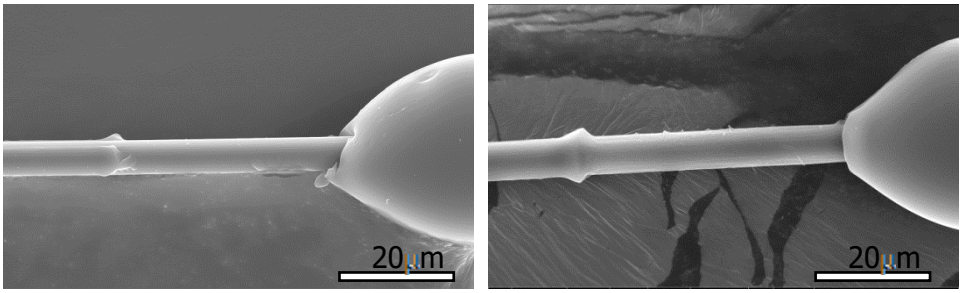

(a) DB (vCF) (b) CB (I20S2H3)

Fig. 7.

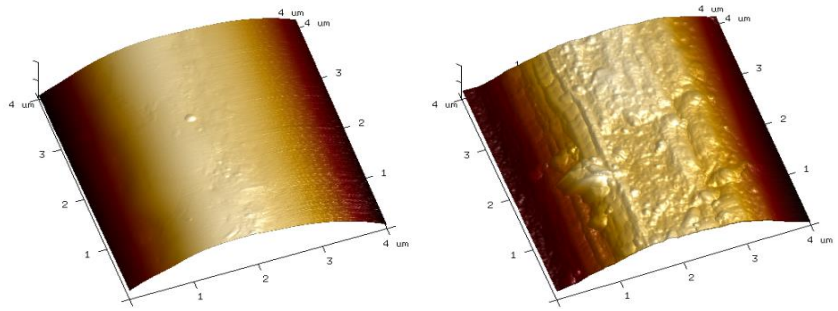

(a) vCF (b) I20S2H3

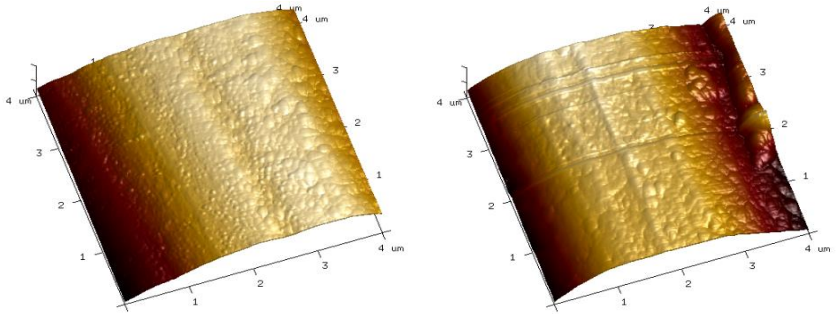

(c) I20S2H3T40 (d) I20S2H3T60

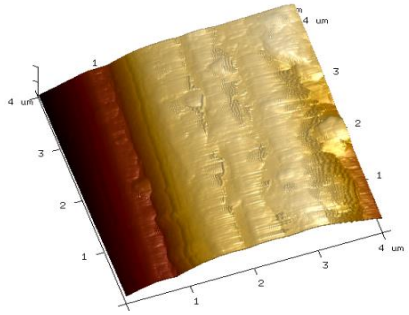

(e) I20S2H3T75

Fig. 8.

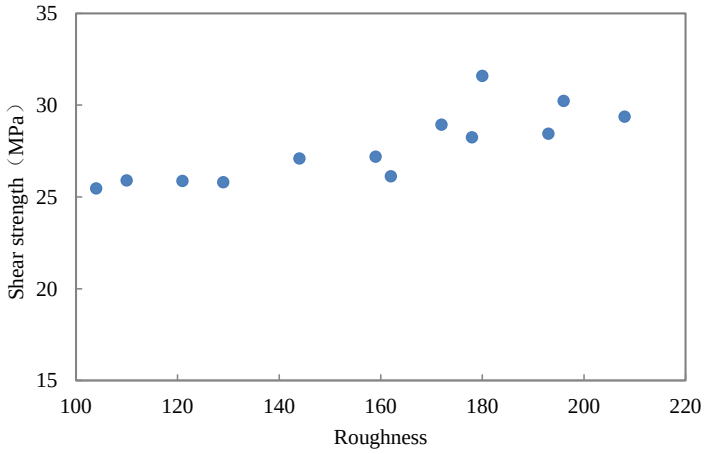

563

564 Fig. 9.

565

566

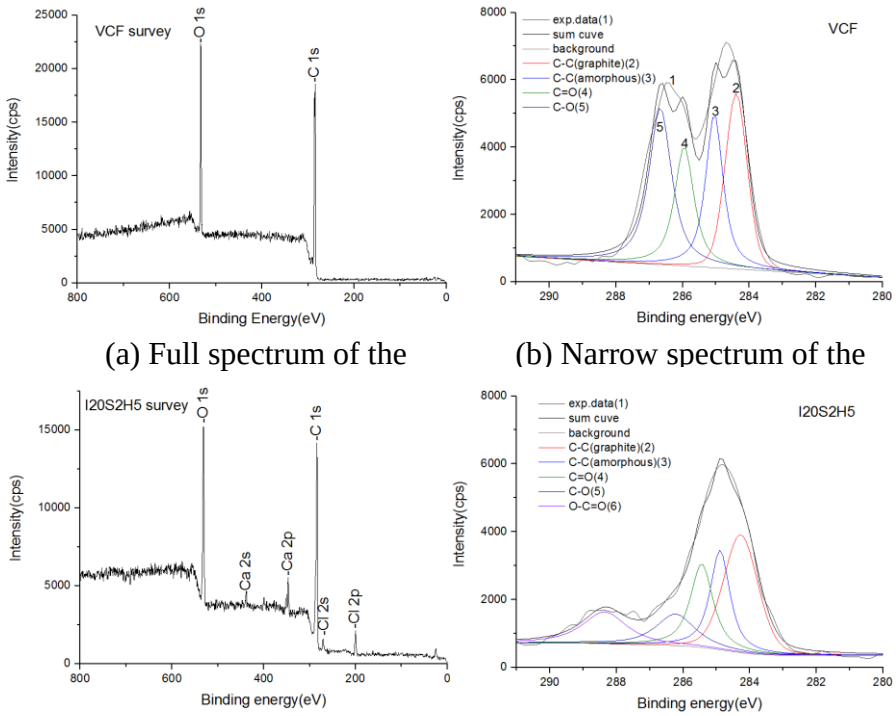

(a) Full spectrum of the (b) Narrow spectrum of the

(c) Full spectrum of the rCFs from I20S2H5

(d) Narrow spectrum of the rCFs from I20S2H5

567

568 Fig. 10.

List of tables

598 Table 1. (Unit: %)

Cement	Silicon powder	High-molecular polymer	chopped CFs	Defoaming agents	Superplasticizer	Water
51.49	5.72	11.44	5.15	0.28	0.17	25.75

599

600

601 Table 2.

Specimens	Current (mA)	NaCl (%)	HNO_3 (g/L)
I20S2H0	20	2	0
I20S2H1	20	2	1
I20S2H3	20	2	3
I20S2H5	20	2	5
I20S3H0	20	3	0
I20S3H1	20	3	1
I20S3H3	20	3	3
I20S3H5	20	3	5
I40S2H0	40	2	0
I40S2H1	40	2	1
I40S2H3	40	2	3
I40S2H5	40	2	5
I40S3H0	40	3	0
I40S3H1	40	3	1
I40S3H3	40	3	3
I40S3H5	40	3	5

602

603

604

605

606 Table 3.

Specimens	Current (mA)	NaCl (%)	HNO_3 (g/L)	Temperature (°C)
I20S2H3T40	20	2	3	40
I20S2H3T60	20	2	3	60
I20S2H3T75	20	2	3	75
I40S2H3T40	40	2	3	40
I40S2H3T60	40	2	3	60
I40S2H3T75	40	2	3	75

607
608
609
610
611
612
613
614
615
616
617
618
619
620
621
622
623
624
625
626
627

628 Table 4.

Specimens	Mass of rCFs (mg)	Compared to vCFs (%)	Hardness
vCF	841	---	---
I20S2H0	0	0	HB
I20S2H1	233	27.71	5B
I20S2H3	598	71.11	9B
I20S2H5	516	61.36	<< 9B
I20S3H0	0	0	2B
I20S3H1	512	60.88	7B
I20S3H3	591	70.27	9B
I20S3H5	494	58.74	<< 9B
I40S2H0	0	0	2B
I40S2H1	286	34.01	9B
I40S2H3	574	68.25	9B
I40S2H5	496	58.98	<< 9B
I40S3H0	0	0	5B
I40S3H1	483	57.43	9B
I40S3H3	565	67.18	9B
I40S3H5	485	57.67	<< 9B
I20S2H3T40	772	91.80	<<9B
I20S2H3T60	688	81.81	<<9B
I20S2H3T75	665	79.07	<<9B
I20S2H3T40	841	77.65	<<9B
I20S2H3T60	653	75.03	<<9B
I20S2H3T75	631	72.89	<<9B

629 Note: The hardness levels of the pencil hardness tester (from low to high) are as follows: 9B-8B-7B-6B-
630 5B-4B-3B-2B-1B-HB-F-H-2H-3H-4H-5H-6H-7H-8H-9H
631

632 Table 5.

Specimens	Tensile strength (MPa)	Compared to vCF (%)	IFSS (MPa)	Compared to vCF (%)	Failure modes	Droplet diameter (μm)	Average roughness (Ra)/nm
vCF	3588	-	27.09	100	DB	46.12–51.35	144
I20S2H1	3072	85.62	31.58	116.57	DB	44.68–50.32	180
I20S2H3	2974	82.89	29.37	108.42	CB	42.26–51.09	208
I20S2H5	2391	66.64	25.46	93.98	CB	43.68–51.03	104
I20S3H1	3001	83.64	28.44	104.98	DB	46.12–50.85	193
I20S3H3	2898	80.76	30.22	111.55	CB	46.95–50.85	196
I20S3H5	2301	64.13	25.90	95.61	CB	42.34–50.54	110
I40S2H1	3049	84.98	28.24	104.25	DB	43.81–50.73	178
I40S2H3	2953	82.30	26.12	96.42	CB	42.57–47.30	162
I40S2H5	2260	62.99	25.87	95.50	CB	43.34–50.85	121
I40S3H1	2987	83.25	28.93	106.79	DB	48.49–51.81	172
I40S3H3	2944	82.05	27.18	100.33	CB	42.57–49.67	159
I40S3H5	2162	60.26	25.79	95.20	CB	42.57–44.94	129
I20H3S2T40	2965	82.64	22.78	84.09	DB	42.64–47.32	134
I20H3S2T60	3118	86.90	28.45	105.02	DB	42.57–49.67	168
I20H3S2T75	3214	89.58	25.11	92.69	DB	45.68–50.86	184
I40H3S2T40	2881	80.30	23.51	86.78	DB	41.39–49.67	149
I40H3S2T60	2949	82.19	26.75	98.74	CB	44.94–52.03	169
I40H3S2T75	2960	82.50	24.29	89.66	DB	43.76–48.49	192

633

634

635

636

637

Table 6. (Unit: %)

Specimens	C	O	Cl	N	Si	Ca	O/C	C-C[1]	C-C[2]	C=O	C-O	C-Cl	O-C=O
vCF	79.3	20.7	0	0	0	0	0.261	27.3	23.8	19.9	29	0	0
I20S2H1	68.2	25.2	1.4	0	3.4	1.8	0.370	34.4	18.4	15.8	18.8	0	12.6
I20S2H3	69.7	26.9	2.5	0	0	0.9	0.386	32.7	16.7	17.5	16.5	0	16.6
I20S2H5	69.1	25.9	2.4	0	0	2.6	0.375	32.3	16.1	18.8	17.2	0	15.6
I20S2H3T40	66.8	28.4	4.8	0	0	0	0.425	28.3	16.6	16.8	12.5	8.2	17.7
I20S2H3T60	64.6	27.7	2.4	2.8	1.8	0.6	0.429	22.9	22.0	20.6	18.3	0	16.2
I20S2H3T75	63.7	25.9	1.9	5.2	2.6	0.7	0.407	29.9	21.5	19.7	13.6	0	15.3

638

639